forum acusticum 2026
8-12 September · Graz, Austria

A COMPARATIVE STUDY OF 3D-PRINTED CELLO BRIDGES. WHICH ONE COMES CLOSEST TO THE ORIGINAL?

Alexander Mayer[1], Montserrat Pàmies-Vilà[1]

[1] *Department Music Acoustics – Wiener Klangstil, mdw – University of Music and Performing Arts Vienna, Vienna, Austria*

Abstract

The differences between 8 3D-printed bridges, which were fabricated using various 3D-printing technologies, materials and internal structures, were explored and compared to the original wooden cello bridge. Input admittance measurements were used to investigate how the different bridges affect the resonance characteristics of the bridge–body system. These measurements were obtained using an automated impact hammer system mounted on a robotic arm. This allowed the fragile impact hammer to be moved to a safe position while the bridge was being interchanged, and ensured highly reproducible excitations. The response was captured using two accelerometers attached to either side of the bridge under test. A laser and camera system assisted with the repositioning of the bridges and accelerometers. During six measurement sessions all 9 bridges were tested, with 20 impact measurements per bridge. The high number of repetitions and exchange sequences was intended to identify the actual influence of the material on the measurements and to exclude differences caused by repositioning on the instrument. Input admittance, coherence and speed of sound within the tested bridges are compared amongst materials. The findings provide a foundation for the further development of a 3D-printed sensor-equipped bridge.

Keywords: *cello bridge, admittance measurements, music acoustics, 3D printing*

1. Introduction

Input admittance measurements are widely used to characterise the vibrational behaviour of bowed string instruments. By considering admittance as a function of frequency, it is possible to identify resonant peaks that correspond to the natural modes of the instrument's bridge–body system. These measurements have proved reliable for studying structural dynamics and play an important role in instrument research and manufacturing [1]. The soundpost side of the bridge mainly supports strings A_3 and D_3, whereas the bass-bar side supports strings G_2 and C_2, creating asymmetrical mechanical conditions that affect vibration transmission. At low frequencies, typically between 170 Hz and 600 Hz for cellos, the admittance curve reveals prominent resonances, while below approximately 200 Hz the bridge motion is constrained by the soundpost that couples the top and back plates [2].

Recent advances in additive manufacturing have opened new possibilities for investigating instrument components with customised geometry and material properties [3]. In particular, 3D printing enables fast prototyping and simplifies the integration of sensory elements into the designs. This study was carried out with the primary motivation to find the optimum material and internal structure combination for further development of a sensor bridge [4]. To that aim, several 3D-printing techniques were applied to produce 8 cello bridges following the geometry of a wooden bridge (Fig. 1). The paper aims to describe the influence of material and internal structure on the vibrational characteristics of the instrument while addressing the topic of reproducibility of measurements.

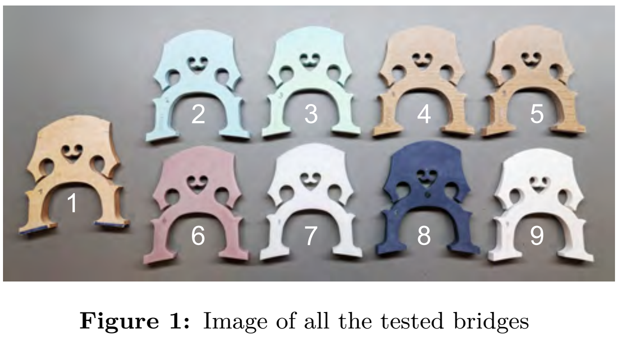

Figure 1: Image of all the tested bridges

Corresponding author: *mayer@mdw.ac.at.*

2. Methodology

The study considers four 3D-printing materials, variations of internal structure, as well as different fabrication technologies. The vibrational characteristics of the bridge–cello system were captured for each bridge via impact hammer measurements.

2.1. Fabrication of 3D-printed bridges

Four 3D-printed materials were choosen: polylactic acid (PLA), PLA/PHA wood fibre composite, photopolymer resin and Digory®[1]. For the first three materials, two infill conditions were tested. The fabrication method and weights of the different bridges are shown in Table 1. The production process utilised two different 3D printing technologies: fused deposition modelling (FDM) and masked stereolithography (MSLA). The 3D model was drawn according to the original wooden bridge (bridge 1). As is common practice for instrument makers, the feet of all bridges were adjusted to the curvature of the top plate of the cello using typical instrument makers' tools.

Table 1: Material and weight of the bridges

#	Material	Fabrication	Weight
1	Maple wood	Wood craft	23.6 g
2	PLA	FDM - infill 40%	33.5 g
3	PLA	FDM - infill 99%	44.9 g
4	PLA - wood	FDM - infill 40%	27.3 g
5	PLA - wood	FDM - infill 99%	36.4 g
6	Resin	MSLA - solid	44.7 g
7	Resin	MSLA - solid	44.9 g
8	Resin	MSLA - hollow	30.9 g
9	Digory	SLA - solid	59.8 g

For bridges 2 to 5, the slicing software Creality Print 6.3 was used to generate the print-data (G-Code) for printing in FDM. In the process-settings "Strenght" the setting "Wall loops" was set to 6, resulting in a wall thickness of 2.4 mm. Two versions of G-Code were generated, one with the value of "sparse infill density" set to 99 % in one case and 40 % in the other. As sparse infill pattern, the "Grid" option was used for all four variations. The Creality Ender-5 Max 3D printer was used for the production of bridges 2 to 5. Bridges 2 and 3 were printed using the Matte PLA Filament by eSun 3D. Bridges 4 and 5 were made of colorFabb woodFill - PLA/PHA including fine pine fibres.

Models 6, 7 and 8 were sliced with the free software CHITUBOX Basic and produced on a Saturn (1st gen.) LCD/MSLA printer from Elegoo, using Siraya Tech's Fast ABS-like resin in different colours. The post-curing process was carried out on a curing device by FormLabs (Form Cure), with the temperature set to "off" and a curing time of 30 minutes. For bridge 8, the 3D model was revised to ensure that a hollow yet stable structure is retained (see Figure 2). After printing, measures were taken to allow any uncured resin to drain away through holes in the shell. These holes were afterwards sealed with the resin and cured with a mini UV-flash-light.

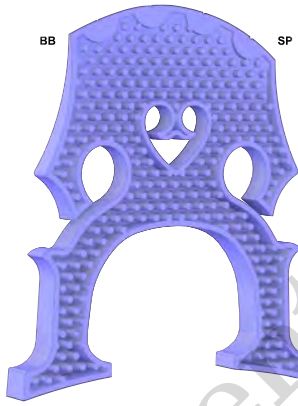

Figure 2: A cross-sectional 3D model of the modified hollow bridge (bridge 8).

2.2. Measurement system

A beginner-level 4/4 cello by Thomann was mounted fixed on a stand, as used in previous setups [5], [6]. A UR5e robotic arm by Universal Robots was positioned in front of the instrument. Both components were fastened on an optical table. Rather than a bow, the robotic arm was fitted with an scalable automatic modal hammer (SAM1 by NV-Tech-Design in conjunction with the PCB model 086E80 impact hammer) to provide controlled excitation through impact. A webcam was also mounted on the end effector of the robot to monitor the position of the bridge on the cello. To obtain the instrument's response, an accelerometer (PCB Model 352C23) was attached on the bridge on the side of the base bar (BB) and another on the side of the sound post (SP) as indicated in Fig. 3. An additional reference accelerometer was located above the f-hole on the treble side of the instrument.

2.3. Towards assuring reproducibility

Since this test requires replacing the bridge frequently, various systems were combined in order to achieve the highest possible reproducibility.

The impact hammer and webcam (see 1 and 2 in Fig. 3) were moved by the robotic arm into a safe position during the bridge-exchange process, the tuning process and if a human playing test needed to be carried out. The robot would then bring the measurement system back to the exact position. Since for each bridge exchange the accelerometers had to be reattached, the pictures from the webcam were used in combination with the Stop Motion Studio Pro software. This software enabled a live camera image to be displayed over a previously recorded image, while their level of transparency could be adjusted. In addition, a laser beam pointed to the spot of the SP accelerometer, and two laser beams drew lines on the instrument body to indicate the position of the feet. These three

[1] Digory® by Eburo (photopolymer resin imitating ivory): https://eburo.at/digory/ Accessed: March 2026

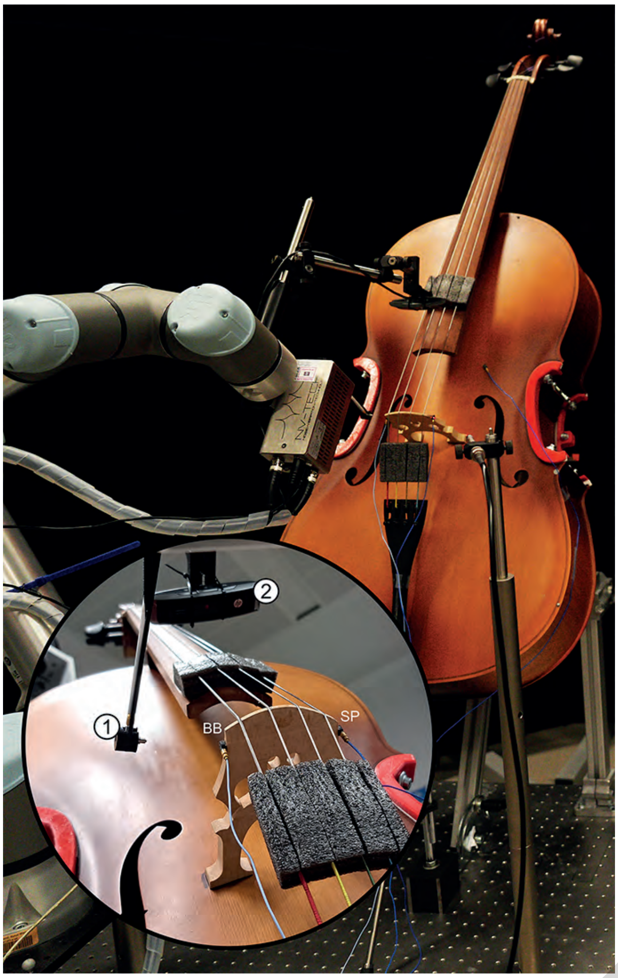

Figure 3: The setup: automated impact hammer (1), webcam (2) and two accelerometers (PCB Model 352C23) attached to the bridge at positions BB and SP.

laser markers in conjunction with the impact hammer tip and the live camera image helped to position the bridges on the cello. The temperature and relative humidity variations are reported in Table 2.

Table 2: Temperature and relative humidity per day

Day	Date	Temp. [°C]	Rel. Hum. [%]
1	21.10.	22.4	39.5
2	22.10.	22.5	48.4
3	23.10.	21.7	51.1
4	24.10.	21.6	42.9
5	11.11.	23.0	37.6
6	25.11.	20.8	38.9

For a quicker and more finger-friendly tuning process, the screws of the fine tuners were replaced by metric M3 hexagon socket head screws, which allowed to change the setting using a small electric screwdriver. The friction pegs were replaced by Wittner Finetune-Pegs Model No. 272111S04. All measurements were taken with the strings dampened at two positions (see the black foam blocks between the strings in Fig. 3). The strings were tuned carefully after each bridge replacement. Standard Thomastik Infeld (Dominant) strings were used, which means that a consistent string quality can be expected. As the A string is the thinnest, it had to be replaced most frequently.

2.4. Data acquisition

The signal from the impact hammer as well as from the accelerometers was connected to an 8-channel signal conditioner, Model 483C05, from PCB. This conditioner also served as an ICP® power source. The data acquisition device, the USB-6421 mioDAQ series from National Instruments (NI) connected via USB-C to a PC, provided 4-channel recording with a rate up to 1 MS/s. A custom recording software was written in NI LabView. This software stored the captured time-domain signals in a text file in SI units. The software started recording into the file as soon as a rising edge of the impact-hammer channel occurred and stopped the recording after a set number of recording buffers. The LabView GUI featured a display of the captured time-domain signals and also provided a preview of the current admittance data. The software also utilised the DAQ's output capabilities to trigger the SAM1 impact hammer. The user could set the number of impact repetitions on demand, thereby determining the total number of measurements to be stored in separate files.
Following a series of test measurements, the instrument was excited 10 times after each bridge exchange and the signals were recorded at a sampling rate (f_s) of 100 kHz. To obtain a higher resolution for comparisons in the time domain, a further 10 measurements were then taken at a f_s of 500 kHz. All measurements and software discussed in this paper are available in Zenodo [7].

2.5. Data processing

In this study, the tested bridges are compared in terms of the input admittance curve and the speed of the wave propagation in the material. Furthermore, coherence tests are provided to relate input and output signals in the frequency domain.
For the admittance calculation, the accelerometer at the base bar (BB) side, as well as the impact hammer signal (also at position BB) are chosen at a f_s of 100 kHz. First, the FFT of both signals is calculated (length of 2^{16} samples; see Matlab code in [7]), the acceleration signal is then integrated once to obtain the velocity signal in the frequency domain. The input admittance is calculated as the ratio between velocity and force displayed in dB.
The time signals of the acceleration recordings at a f_s of 500 kHz, measured at the sound-post a_{SP} and bass-bar a_{BB} side of the nine bridges, are used to calculate the speed of the longitudinal wave propagation within the material, considering the distance of 63.5 mm between the accelerometers on both sides of the bridge. The delay in samples between the two signals is indicated by the arrows in Figure 4 (bridges 1 and 3; day 3).

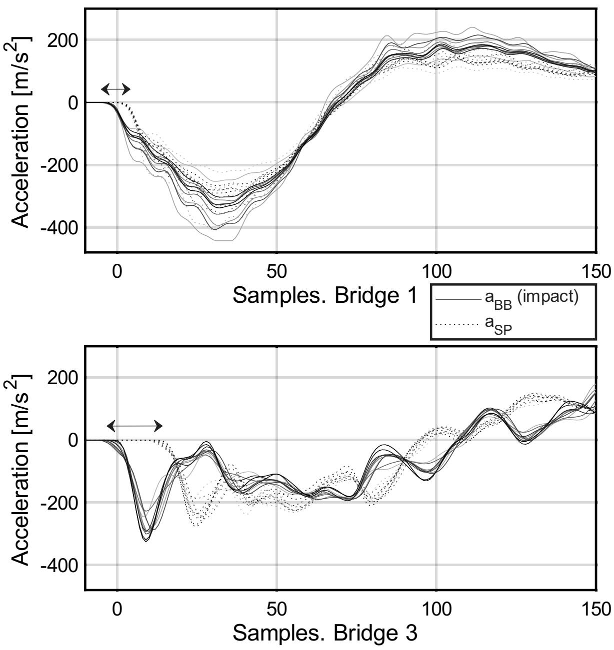

Figure 4: Acceleration measured at the sound-post side a_{SP} and bass-bar side a_{BB} of bridges 1 and 3 on day 3; 10 impact-hammer excitations at the BB side.

The coherence function is used to evaluate the quality of the data (orange curves in Figure 7), identifying causality between the measured output (acceleration a_{BB}) and the input signals (impact force) [8], [9]. To calculate this indicator, the power spectra $S_{xx}(f)$ of the input signal, the power spectra $S_{yy}(f)$ of the output signal, as well as the cross power spectrum $S_{xy}(f)$, all averaged across all trials ($k = 1...K$), are calculated. The coherence $C_{xy}(f)$ is given by:

$$C_{xy}(f) = \frac{|\frac{1}{K}\sum_{k=1}^{K} S_{xy}^{(k)}(f)|}{\sqrt{\frac{1}{K}\sum_{k=1}^{K} S_{xx}^{(k)}(f)} \cdot \sqrt{\frac{1}{K}\sum_{k=1}^{K} S_{yy}^{(k)}(f)}}$$

3. Results

3.1. Speed of wave propagation in the material

The values obtained for the speed of the wave propagation within the material for the 3D-printed bridges are shown in Fig. 5. For bridge 1, made of maple wood, the measured value is 8015.9 ± 1160.3 m/s (mean $\pm$ standard deviation). Bridge 1 also exhibits the greatest quantisation error (approx. 20%), due to a narrow time delay between the signals (accelerometers at SP and BB side of the bridge) of about 3–5 samples at 500 kHz f_s (see top of Fig. 4). A set of recordings at a f_s of 10^6 Hz corroborated the results. Variations in the speed of the longitudinal wave in maple wood around 4000 m/s to around 5500 m/s have been reported in the literature [10].

For all 3D-printed materials (Fig. 5), the quantisation error is minor (approx. 6%) compared to that in the wooden bridge, since the delay between the two

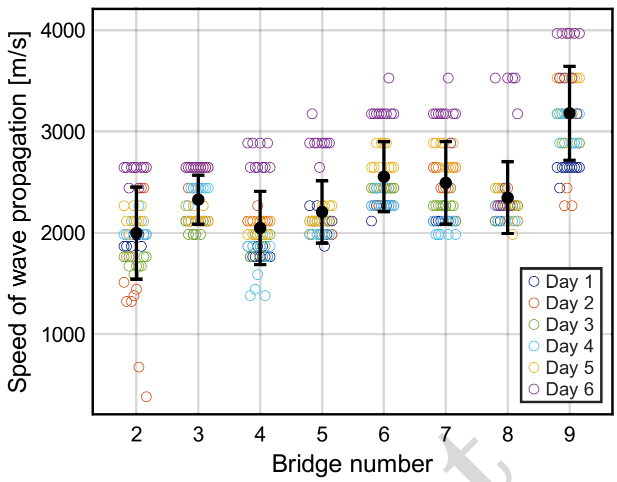

Figure 5: Speed of longitudinal wave propagation in the different 3D-printed materials: raw data overlapped by the corresponding error plot (mean and standard deviation). Bridge 1 (wooden – not shown) is 8015.9 ± 1160.3 m/s.

accelerometers is around 15–17 samples (at a f_s of 500 kHz). The mean speed of wave propagation for the PLA bridges (bridges 2–5) is 2135.1 ± 371.7 m/s, whereas it is slightly higher for the photopolymer resin ones (bridges 6–8): 2464.8 ± 377.9 m/s. These values are consistent with those reported in the literature [11]: PLA at 2246 m/s, and photopolymer resin at 2427 m/s. Regarding the differences among days, day 6 seems to show higher values than the previous days, which may be due to the non-linear response at different impact forces, or to the conditions in the room. Yet, it does not correspond to any consistent change in the laboratory conditions (Table 2).

3.2. Input admittance comparison

Figure 6 plots the admittance magnitude per bridge averaged across repeated measurements (60 measurements). On the left, the bridges are ordered with increasing weights from top to bottom. The shaded zones indicate the range per frequency beam (maximum and minimum across all measurements). On the right of Fig. 6, several comparisons are shown.

The effect of material weight, which was not entirely unexpected, can be confirmed by this analysis: increasing weight shifts the resonant frequencies down. This is clear for the first and second resonant peaks, marked with black dashed lines (Fig. 6a). As observable in Fig. 6b, the admittance peak levels of bridge 9 are clearly below those of all other bridges. This is, as expected, a consequence of the high weight of this bridge.

Comparing the original bridge to the one with the closest weight (bridge 1 vs. bridge 4), Fig. 6c shows great alignment of frequency resonances below 500 Hz. In the range between 500 Hz and 1600 Hz, fewer similarities are found. This range might correspond to the bridge hill [12], [13] – yet this could not be confirmed. Between aprox. 1600 Hz and 10 kHz, the admittance

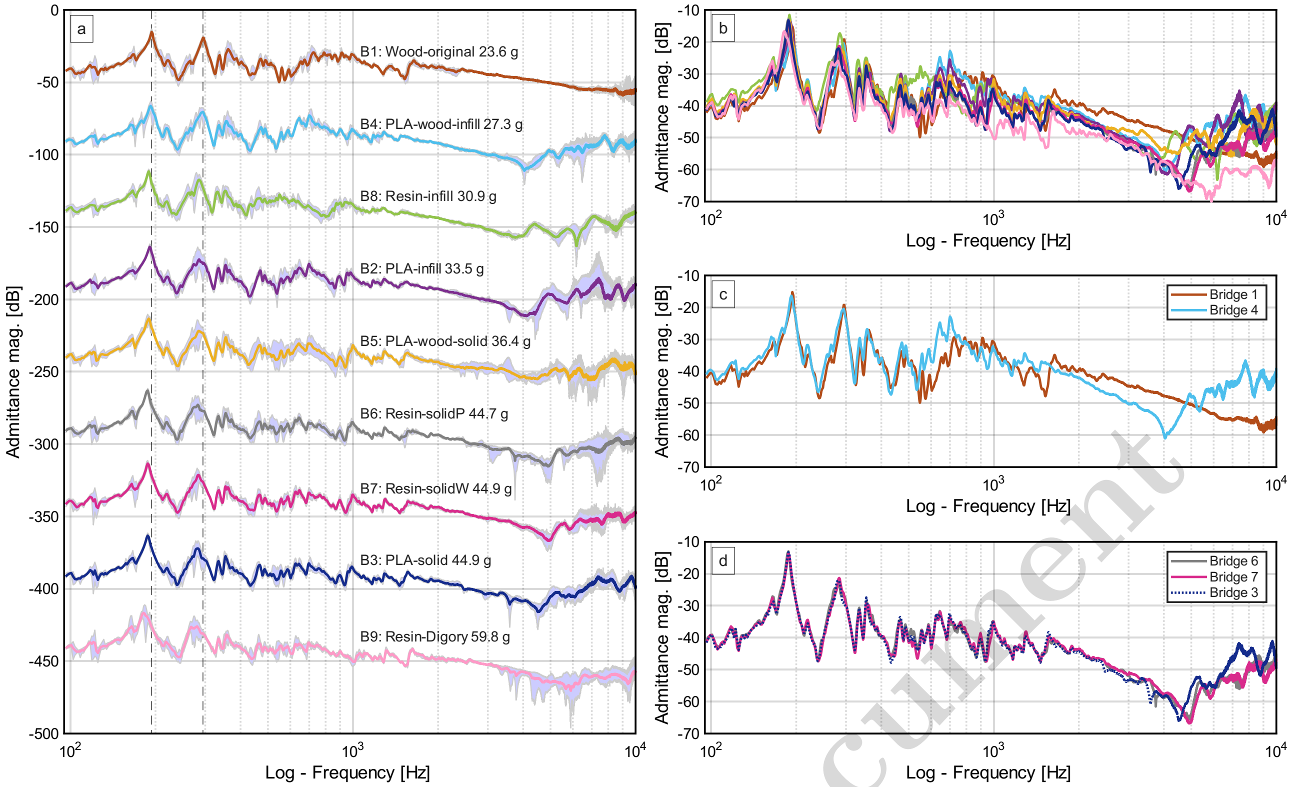

Figure 6: a) Mean admittance curves ordered according to bridge weight, separated by 50 dB for visualisation ($f_s = 100$ kHz). The shaded zone is given by the maximum and minimum values per frequency beam among all measurements. Vertical dashed lines indicate the frequency of the first and second resonance peaks of bridge 1; b) Mean admittance curve of all bridges; c) Original bridge (1) vs. the most-similar 3D-printed bridge (4); d) Three 3D-printed bridges with the most similar weight (3, 6, 7).

curves show different slopes: bridge 4 decays more steeply, while bridge 1 remains comparatively flatter. All 3D-printed bridges share the tendency of bridge 4 (Fig. 6b).

Similarly, when comparing heavier bridges with almost the same weight (bridges 3, 6 and 7, Fig. 6d), a clear alignment is given up to 5000 Hz, both in the frequency and in the magnitude axes, independently of the material used. This was predictable for bridges 6 and 7, which were manufactured identically using resin; but not for bridge 3, which is made of PLA instead.

3.3. Repetitions and coherence

Across all measurements per bridge, coherence remains close to 1 in the range between 100 Hz and 1700 Hz for all bridges (see for example 10 repetitions for day 1 and bridge 1 in Fig. 7), indicating high data quality and strong repeatability of the measurements. Similar results were reported in [14]. Comparing all recording sessions, the bottom of Fig. 7 shows the coherence across all 60 measurements for one bridge. Even though this plot considers several days, the coherence still remains above 0.8 for most of the frequency spectrum. Similar results are observed for all tested bridges [7].

4. Conclusions

The study presents an exploratory analysis of potential 3D-printable materials for cello bridge prototyping. Comparing input admittance and propagation velocity provides a strong foundation for further analysis. All 3D-printed bridges show wave propagation speeds around 2000–4000 m/s, with higher values observed for resin than for PLA materials. General trends in the admittance curves appear to be primarily attributed to weight, with lighter bridges resembling the original wooden bridge below 500 Hz. Heavier bridges display lower admittance magnitudes, which might result in dampened sound. Yet, in a preliminary bowing test conducted with a professional musician, all bridges proved to be suitable for playing the cello. According to the musician's sensation during playing, the PLA-wood bridge with 40% infill (bridge 4) most closely resembled the original bridge, corroborating the admittance comparison results. Further playing tests are necessary to determine the material parameters that influence response and playing feel.
Given the considerable technical expertise, meticulous handling, and extensive number of measurements involved, the findings are considered highly reliable. Despite our best efforts to make the measurement conditions reproducible, some issues must be acknowledged. When fitting the bridge, close attention was

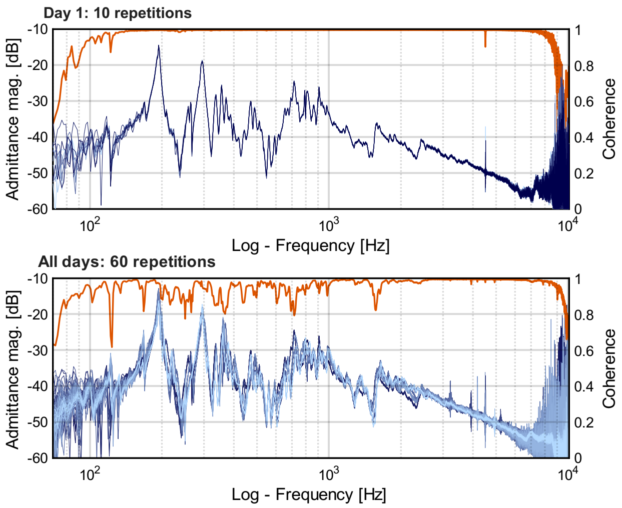

Figure 7: Admittance and coherence of bridge 1 (top) for 10 repetitions on the first day, and for bridge 1 over all days and repetitions (bottom).

required to ensure the feet were placed correctly on the top plate. Tuning the strings also required careful monitoring of any bridge tilt. By tuning using the tuning pegs and the fine-tuners as a counterpart, this was largely achievable. Nevertheless, it cannot be excluded with absolute certainty that a slight tilt developed during preparation before the measurements, causing one side of the bridge feet to lift slightly. We attribute this behaviour to differences in sliding resistance between the bridge materials and the strings, as well as to differences in bridge flexibility. This could explain the measurement differences observed in measurements taken on different days for the same bridge. For further studies, measurements should not be taken immediately after tuning the strings. Instead, some time should be allowed for the string-bridge system to settle, after which any necessary readjustments should be made. Additionally, further wave propagation measurements using different impact forces could clarify non-linear material properties.
Overall, the study identifies a potential candidate for further development of sensorised 3D-printed bridges: the admittance curve of bridge 4 is the closest to the original. The importance of carefully repositioning the measurement setup and the bridge to minimise variability in repeated measurements is emphasised. Such a study complements traditional lutherie by exploring how additive manufacturing can facilitate systematic studies of the relationships between design and properties in string instruments.

5. Acknowledgements

The authors would like to thank Thaddäa Rath from Eburo for providing a 3D-printed bridge in Digory® using the model of this study.

References

[1] A. Zhang and J. Woodhouse, "Reliability of the input admittance of bowed-string instruments measured by the hammer method," *J. Acoust. Soc. America*, vol. 136, no. 6, pp. 3371–3381, 2014.

[2] A. Zhang, J. Woodhouse, and G. Stoppani, "Motion of the cello bridge," *J. Acoust. Soc. America*, vol. 140, no. 4, pp. 2636–2645, 2016.

[3] J. Haines-Eitzen, *3D printed cello bridges*, `https://www.youtube.com/watch?v=nvkYhKqw_7Y`, YouTube video of the Oberlin Acoustics Workshop (accessed April 2026), 2023.

[4] A. Mayer, M. Pàmies-Vilà, and V. Chatziioannou, "Ein Roboterarm spielt Cello," *OCG Journal*, no. 4, pp. 16–19, 2023.

[5] A. Scheiblauer, A. Mayer, and M. Pàmies-Vilà, "Investigating the cello position, bow motion and cellist posture using motion capture," in *Proc. Meetings on Acoustics*, Vienna, Austria, 2022.

[6] M. Pàmies-Vilà, A. Mayer, E. Matusiak, and V. Chatziioannou, "A method for the reproduction of cello bow kinematics using a robotic arm and motion capture," *Acta Acustica*, vol. 8, p. 45, 2024.

[7] M. Pàmies-Vilà and A. Mayer, *Dataset to: "A Comparative Study of 3D-Printed Cello Bridges. Which One Comes Closest to the Original?"* Zenodo, 2026. DOI: `10.5281/zenodo.20797149`.

[8] P. Avitabile, "Experimental modal analysis," *Sound and Vibration*, vol. 35, no. 1, pp. 20–31, 2001.

[9] P. Avitabile, "Modal space-in our own little world," *Experimental Techniques*, vol. 36, no. 3, pp. 1–2, 2012.

[10] A. Danihelová, Z. Vidholdová, T. Gergel', L. Spišiaková Kružlicová, and M. Pástor, "Thermal modification of spruce and maple wood for special wood products," *Polymers*, vol. 14, no. 14, p. 2813, 2022.

[11] D. Ma, R. Gao, M. Li, and J. Qiu, "Mechanical and medical imaging properties of 3D-printed materials as tissue equivalent materials," *J. Appl. Clin. Med. Phys.*, vol. 23, no. 2, e13495, 2022.

[12] E. Jansson and B. Niewczyk, "On the acoustics of the violin: Bridge or body hill," *J. Catgut Acoust. Soc. Series*, vol. 2, no. 3, pp. 23–27, 1999.

[13] J. Woodhouse, "On the "bridge hill" of the violin," *Acta acustica united with acustica*, vol. 91, no. 1, pp. 155–165, 2005.

[14] E. Maestre Gómez, G. Scavone, and J. Smith, "Digital modeling of bridge driving-point admittances from measurements on violin-family instruments," in *Proc. SMAC 2013*, Stockholm, Sweden, 2013.